Journal of South American Earth Sciences 100 (2020) 102537

Contents lists available at ScienceDirect

Journal of South American Earth Sciences

journal homepage: www.elsevier.com/locate/jsames

Geology and structural controls of the Ag–Sn–Zn Pirquitas deposit, northwestern Argentina

Fernanda Monteiro Passamani[a], Everton Marques Bongiolo[b,*], Felipe Nepomuceno de Oliveira[c], Reiner Neumann[d]

[a] Brazilian Navy Hydrographic Center (CHM), Directorate of Hydrography and Navigation (DHN), Brazilian Navy, Brazil
[b] Instituto de Geociências, Universidade Federal do Rio Grande do Sul (UFRGS). Av. Bento Gonçalves 9500, Agronomia, CEP 90650-001, Porto Alegre, Brazil
[c] Programa de Pós–graduação em Geologia. Universidade Federal do Rio de Janeiro (UFRJ), Brazil
[d] Center for Mineral Technology (CETEM), Brazil

ARTICLE INFO

Keywords:
Pirquitas deposit
Structural control
Bolivian belt

ABSTRACT

Pirquitas is a polymetallic silver, tin, and zinc deposit, located in the Altiplano–Puna plateau, northwestern Argentina. The mineralization occurs in veins and hydrothermal breccia hosted in Ordovician meta–sedimentary rocks, but there is a lack of data on the structural geology of the deposit. In this paper we use detailed field mapping accompanied by structural analysis and mineralogy (petrography and XRD) to infer: (i) the mineralization structural controls, (ii) the influence of regional structures on the deposit formation, and (iii) characteristics of the Pirquitas deposit as compared with those from the Bolivian Tin–Silver Belt.

The main stage of deformation observed at Pirquitas is associated with the Late Ordovician–Early Silurian Oclóyic orogeny. However, the ore deposition occurs as recurrent hydrothermal pulses related to the reactivation of Ordovician structures during the upper Miocene Quechua orogeny, which was partially contemporaneous with volcanic activity. The NW–SE and WNW–ESE ore–bearing veins of the Pirquitas deposit represent, respectively, second–order R– and T–fractures associated with major regional–scale, sinistral, brittle shear zones such as the Lípez and the Olacapato–El Toro faults.

Similarities in mineralogy, structural control and association with magmatic activity indicate that Pirquitas is the southernmost deposit of the Bolivian Tin–Silver Belt. As such, subvolcanic intrusions associated with the Granada Volcano and the Coranzuli Caldera that are aligned along regional structures should be investigated by future exploratory works looking for porphyry to epithermal mineralization in the region.

1. Introduction

The Pirquitas deposit is a polymetallic (silver, tin, and zinc) ore deposit located in the Altiplano–Puna plateau, Province of Jujuy, northwestern Argentina. The ore exploration at Pirquitas started on tin placers and changed to underground mining when primary silver, tin, and zinc targets were discovered (Soler et al., 2008). The deposit was exploited as an open pit mine since 2009, and comprised a vein system hosted in Ordovician meta–sedimentary rocks.

Silver Standard Resources Inc. (2011) estimated proven reserves of 48 million ounces of silver at an average grade of 180 g/t, and probable silver reserves of 26 million ounces at 169 g/t, ranking Pirquitas among the largest primary silver ore deposits worldwide. Proven and probable zinc reserves were 93 million pounds at 0.51% and 109 million pounds at 1.03%, respectively. After the discovery of the major new silver, lead and zinc Chinchillas deposit, Silver Standard (now SSR Mining, SSRM) entered into a Joint Venture with the Golden Arrow Resources Corporation, in order to provide infrastructure to the development of Chinchillas. Pirquitas operated until 2017 and is now moving to a reclamation and closure stage.

Based on mineralogical similarities, several authors (e.g., Malvicini, 1978; Paar et al., 2000; Coira et al., 2000) compared the Pirquitas deposit with those of the Bolivian Tin–Silver Belt (BTSB). Although the mineralization in this belt has been associated with mid–Miocene magmatism, no intrusive magmatic body crops out at Pirquitas (Soler et al., 2008). Exploration research developed during the mining activity has suggested the Granada Volcano and the Cerro Galán dome, located 13 km to the north and 12 km to the east of the deposit, respectively, as

* Corresponding author.
E-mail addresses: passamani@marinha.mil.br (F.M. Passamani), bongiolo@ufrgs.br (E.M. Bongiolo), fnepol@gmail.com (F. Nepomuceno de Oliveira), rneumann@cetem.gov.br (R. Neumann).

https://doi.org/10.1016/j.jsames.2020.102537
Received 24 May 2019; Received in revised form 17 February 2020; Accepted 17 February 2020
Available online 10 March 2020

probable intrusions associated with the ore genesis.

The identification of different stages of folding, faulting, and fracturing in mineralized regions is an important step to link tectonic events with ore deposition, location, and distribution. Previous investigations report mostly the sporadic rare associations of ore mineralogy at the studied area. The scarce works on the structural geology of the Pirquitas deposit focused solely on the former open pit area and did not integrate the regional tectonics with the stratigraphic record and mineralogy. This contribution aims to identify structural controls on the ore mineralization at the Pirquitas deposit and its association with regional deformational events, based on detailed field mapping and structural geology analysis. Additional petrography (optical and SEM-EDS) and X-ray diffraction were used in selected samples to identify the ore mineralogy and its relation with vein types. We have gathered those data to put the Pirquitas deposit from a regional perspective, in comparison with those reported at the BTSB.

2. Geological overview

2.1. Geological setting

The Pirquitas deposit is located in an area between 4000 and 4800 m above sea level, at the southernmost Altiplano–Puna plateau. This is the highest plateau in the world associated with a magmatic arc, located in the Central Volcanic Zone of the Andes (CVZ; Fig. 1a), and the highest and extensive plateau outside the Tibet, in the Himalayas. The CVZ is an active volcanic area at the Andean Margin, the western margin of the South American plate. The CVZ comprises the Altiplano–Puna plateau, which is flanked by the Sub–Andean Region (Eastern Cordillera and Sub–Andean thrust belts), Precordillera thrust belt, the Pampean Ranges, and the Santa Barbara system (Isacks, 1988; Allmendinger et al., 1997, Fig. 1a).

The plateau is subdivided into the Altiplano (Spanish for "high plain") and Puna domains, located in the Bolivian and Argentinean territories, respectively. The Altiplano (14–21°S) is a broad flat basin with an average elevation of 3.8 km (Isacks, 1988). The surface of the Altiplano is covered by large salars, Quaternary sediments, locally late Oligocene to Recent volcanic rocks, including Miocene to Pliocene ignimbrites, and sparse exposures of Pre–Cenozoic basement (Allmendinger et al., 1997). The Altiplano is flanked by the well-developed, thin–skinned Sub–Andean thrust belt to the east, while the Puna (22–27°S) is flanked by the thick–skinned Santa Bárbara System (Allmendinger et al., 1997).

The study area is located in the northern part of the Puna domain (Fig. 1a). The Puna domain is characterized by fragmented sedimentary basins, with average elevation nearly 1 km higher than the Altiplano (Isacks, 1988). The higher relief has been attributed to thermal uplift caused by the more significant thinning of the lithosphere beneath the Puna, as a result of the variations in geometry of the subducted Nazca Plate (Whitman et al., 1996).

The genesis of the polymetallic mineralizations of the Pirquitas deposit has been interpreted as the southernmost manifestation of the intrusion–related Bolivian Tin–Silver Belt (e.g., Turneaure, 1971; Sillitoe et al., 1975; Malvicini, 1978; Sureda et al., 1986). The BTSB ore

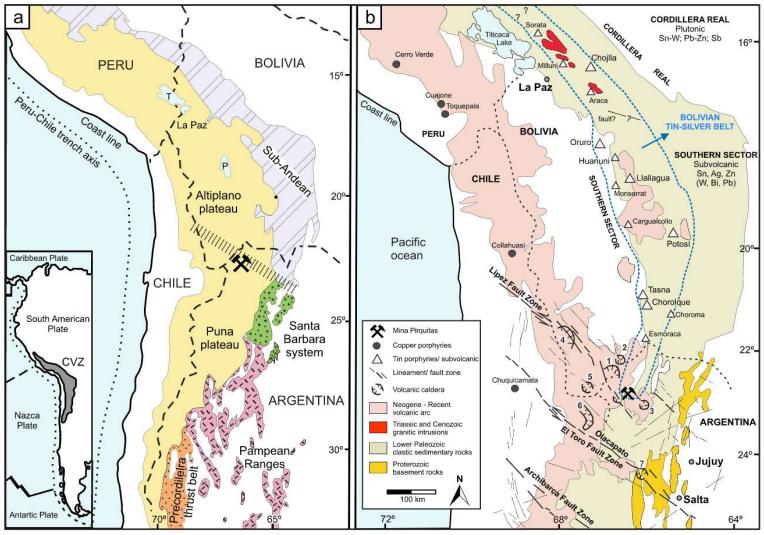

Fig. 1. Regional geology of the Altiplano–Puna plateau. (A) Location of the Pirquitas deposit in the northern Puna, northwestern Argentina, near the NW–SE transition between Puna and Altiplano domains (yellow; transition is the hachured area). The Central Volcanic Zone (CVZ, grey zone on the inset map) also includes the Sub–Andean (purple) and Precordillera (orange) fold and thrust belts, Pampean Ranges (pink) and Santa Barbara system (green). P – Poopó, and T – Titicaca lakes, and ocean in blue. Based on Isacks (1988) and Allmendinger et al. (1997). (B) Location of the Pirquitas deposit in the southernmost sector of the Bolivian Tin–Silver Belt (BTSB). Granitic intrusions occur in the Cordillera Real while porphyry–subvolcanic deposits are related to the Southern Sector. Main WNW lineaments that cut across the Puna region are represented by the Lipez Fault Zone, Olacapato–El Toro Fault Zone an Archibarca Fault Zone. Number in boxes indicate the main volcanic calderas: 1 – Vilama; 2 – Panizos; 3 – Coranzuli; 4 – Cerro Pastos Grandes; 5 – Cerro Guacha; 6 – La Pacana; 7 – Negra Muerta. Based on Turneaure (1971), Dietrich et al. (2000), Riller et al. (2001) and Caffe et al. (2008). (For interpretation of the references to color in this figure legend, the reader is referred to the Web version of this article.)

deposits (Fig. 1b) are subdivided into (i) the Sn–W Cordillera Real plutonic type, related to a series of granitic batholiths of Triassic age (Sillitoe et al., 1975; McBride et al., 1983), and (ii) the Cenozoic Sn–Ag Southern Sector, with porphyry and epithermal ore associated with shallow intrusive bodies (Turneaure, 1971). Within the Southern Sector, the ages of the ore deposits vary from late Oligocene to the North to upper Miocene to the South (Dietrich et al., 2000). Caffe and Coira (1999) suggested that the metallogenetic epoch for the whole northern Puna region coincides with the mid-Miocene volcanism, between 14 and 11 Ma.

Most of the BTSB deposits are associated with felsic intrusions and volcanic domes (Cunningham et al., 1991; Sillitoe et al., 1998) of granitic or rhyodacitic composition. These fractionated igneous rocks are relatively reduced in the ilmenite series (e.g., Ishihara, 1977), probably reflecting organic carbon content in the underlying meta–sedimentary rocks (Lehmann, 1994). Tin and silver from this area are assumed to be derived mostly from peraluminous magmas, which may have extracted metals from meta–sedimentary country rocks. On the other hand, it may be argued that these magmas have only provided the heat to concentrate ore (Turneaure, 1971).

The middle and upper Miocene volcanism and associated ore deposits of northwestern Argentina have been spatially correlated with several structural features that cut across the Puna region, such as Lipez–Coranzuli and Olacapato–El Toro (e.g., Riller et al., 2001, Fig. 1b). These WNW lineaments are interpreted to be deep crustal Paleozoic structures which have been selectively reactivated as sinistral transcurrent faults in Cenozoic times (Allmendinger et al., 1983; Jordan et al., 1983; Alonso et al., 1984; Salfity, 1985; Chernicoff et al., 2002). On the other hand, NNE-striking structures are Cenozoic sutures between Paleozoic and Precambrian rocks.

The dominant Puna rock types are the Lower Paleozoic clastic sedimentary rocks (Fig. 1b). In the study area, the basement is represented by Early Ordovician successions of metasandstones and metapelites of the Acoite Formation, the uppermost member of the Santa Victoria Group. Bahlburg (1990, 1998) interpreted the Acoite Formation as part of the ca. 2000 m thick "Lower Turbidite System" of the "Puna Turbidite Complex", deposited in the Puna basin.

Regional tectonic reconstructions show that the deposition of sedimentary successions has taken place in the Puna back-arc to foreland basin, between a magmatic arc to the west and the emerging Eastern Cordillera (Bahlburg, 1990, 1998; Bahlburg et al., 1990; Mon and Salfity, 1995; Bahlburg and Hervé, 1997, Fig. 2a). Biostratigraphic data of the Acoite Formation points to early Ordovician ages, near the Tremadocian–Floian boundary (ca. 478 Ma; Voldman et al., 2012). The closure of the Puna basin has been associated with the collision of the Puna basement against the Arequipa–Antofalla allochthonous Terrane during the late Ordovician–early Silurian Oclóyic orogeny (ca. 444 Ma; Bahlburg, 1990; Mon and Salfity, 1995; Bahlburg and Hervé, 1997, Fig. 2b). In the northern Puna, this deformation event led to the development of a west–vergent fold pattern with NNE–trending fold axes and faulting, indicating WNW–ESE shortening (Mon and Hongn, 1987; Bahlburg and Hervé, 1997; Cladouhos et al., 1994).

Thermal studies of metapelitic and metavolcanic rocks of the Ordovician successions (Do Campo et al., 2017) show an E–W trend of the metamorphic zones, from diagenesis/low anchizone in the eastern Puna to high anchizone/epizone to the west. {According to those authors, the secondary mineralogy along this trend and the development of a slaty cleavage characterize the low-grade greenschist metamorphism.

At the Pirquitas deposit, the mid-Miocene is represented by sedimentary and volcanoclastic sequences (Fig. 3) of the Tiomayo Formation, composed of sandstone, mudstone, and conglomerate, interbedded with tuffs and ignimbrites (Coira et al., 2004). The sedimentation took place in an intermontane basin between 18 and 12 Ma filled by fluvial–lacustrine sediments with volcanic contribution, recording the first evidence of the Cenozoic explosive volcanism (Coira et al., 2004; Caffe et al., 2008). A whole–rock K–Ar determination on ignimbrite from the Tiomayo Formation at the Pirquitas region yields an age of 14.9 ± 0.5 Ma (Coira et al., 2004).

During the Neogene, a compressive deformation event took place in the Andes, named the "Quechua Phase" of the Andean orogeny. In the Peruvian Andes, this event is subdivided into three compressive pulses (Benavides–Cáceres, 1999): Quechua I (17 Ma); II (8–7 Ma) and III (5–4 Ma). In northern Puna, strong crustal thickening and shortening occurred during the Miocene, between 15 and 9–10 Ma, and is described in two different phases (Gubbels et al., 1993; Cladouhos et al., 1994; Coutand et al., 2001): i) Miocene shortening appears to have reactivated Cretaceous rift structures as NNE–SSW reverse faults of dip-slip movement and subhorizontal, WNW–ESE (~110°) shortening; ii) relatively minor deformation of the younger phase occurred as normal and strike–slip faults, indicating ENE–WSW shortening and horizontal extension. Balanced cross–sections suggest shortening of ~40–50 km

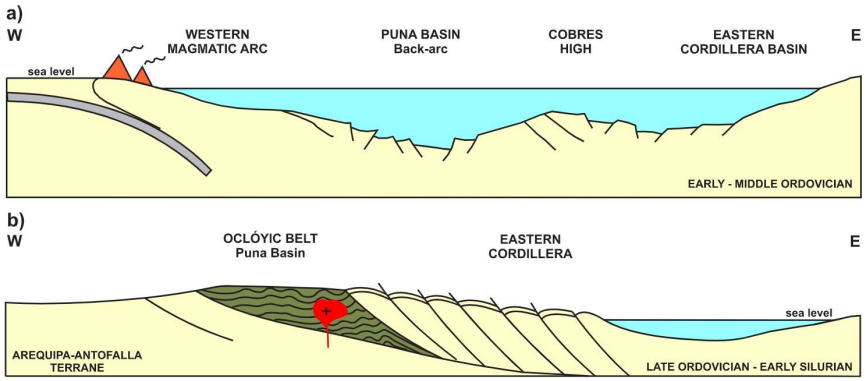

Fig. 2. Structural evolution of the Mina Pirquitas region. (A) Location of the Puna backarc basin (includes the Acoite Formation) between the western magmatic arc and the Cobres High, during the Early–Middle Ordovician. The Cobres High separates the Puna basin from the Eastern Cordillera basin. (B) Deformation of the Puna basin and the Eastern Cordillera after the collision of Arequipa–Antofalla Terrane during the Late Ordivician – Early Silurian Oclóyic Orogeny.

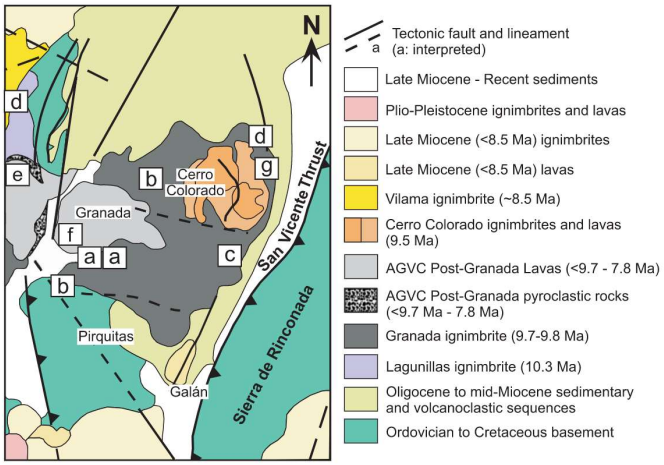

Fig. 3. Geologic map of northern Puna with ages from the Granada Ignimbrite and other Puna Upper Miocene volcanic rocks (Extracted from Caffe et al., 2008). Granada Ignimbrite: (A) $^{40}Ar/^{39}Ar$ 9.76 ± 0.07 and 9.70 ± 0.09 Ma; (B) K/Ar 8.9 ± 0.26 Ma; (C) $^{40}Ar/^{39}Ar$ 10.0 ± 0.2 Ma. Abra Granada volcanic complex units: (D) Lagunillas ignimbrite - $^{40}Ar/^{39}Ar$ 10.25 ± 0.12 Ma; (E) Caucani dome lava – K/Ar 7.9 ± 0.2 Ma. (F) Cerro Granada platform lavas – K/Ar 5.05 ± 0.16 Ma; Post-Granada units: (G) K/Ar 9.5 ± 0.5 Ma.

subperpendicular to the orogen, and elevation of ca. 2000 m on the Puna domain during the Andean deformation (Cladouhos et al., 1994; Coutand et al., 2001).

The upper Miocene transtensive regime favored explosive volcanic activity between ca. 10 and 6 Ma (Caffe et al., 2008, Fig. 3), which resulted in one of the most extensive ignimbrite provinces in the world (De Silva, 1989; Coira and Kay, 2004; Caffe et al., 2008). Pyroclastic deposits associated with this event in the study area are represented by the Granada ignimbrite (ca. 9.8 Ma; Caffe et al., 2008). The Tiomayo Formation and the Granada ignimbrite are flat-lying, but affected by numerous minor (< 2 m offset) strike–slip and normal faults which indicate N–S extension and vertical to E–W shortening (Cladouhos et al., 1994).

2.2. Summary of the previously proposed Pirquitas ore deposit models and processes

The primary ore of Pirquitas is associated with veins and subordinately with hydrothermal breccia emplaced between mid-to upper Miocene (Sureda et al., 1986; Coira and de Brodtkorb, 1995; Slater, 2016). They were historically grouped based on their strike during the mining activity as (1) ESE (100° to 110° – azimuth), which represents more than 60% of the veins, (2) NW (300° to 310°) and (3) ENE (70°–80°).

The mineralized ESE-striking veins are subvertical, dozens to hundreds of meters long and centimeter to meter–thick (30–50 cm on average). Malvicini (1978) identified a first mineralization period (subdivided into early and late stages) and a second one. According to that author, the first period early-stage ore mineralogy consists of pyrite, pyrrhotite, arsenopyrite, and cassiterite. The late stage of this period is characterized by deposition of colloform bands of sphalerite–wurtzite, galena, Ag–sulfosalts, and scarce stannite along fracture zones that crosscut the early veins. The second period is characterized by re–fracturing of first-period mineralized veins-at deeper zones of the ore system, and consists of Bi–sulfosalts, cassiterite, alunite, stannite, and Ag–sulfosalts. Recent studies (Passamani, 2014; Desanois et al., 2019) consider Pirquitas as an epithermal deposit of intermediate to low-sulfidation subtype, with decreasing temperatures from < 400 °C to ca. 150 °C, associated with mixing between magmatic and meteoric fluids, which is usually found in such hydrothermal systems.

Pipes of hydrothermal breccia were described close to the mineralized veins and individualized by Coira et al. (2000) in two groups: (a) polymictic breccia with fragments of sandstone, mudstone, and dacite set in abundant matrix of similar composition that contains also ore–bearing quartz vein fragments; and (b) clast–supported oligomictic breccia, locally mineralized, comprising mostly metapelite (65–70%) and minor metasandstone fragments. Although ground geophysical surveying (i.e., magnetometry and induced polarization) suggested the occurrence of disseminated sulfides in a subvolcanic body or breccia under the open pit area, three drills of ca. 800 m depth did not intersect the expected rocks (Jacobs Engineering Group Inc, 1999).

Hydrothermal alteration assemblage composed of sericite + quartz + pyrite was described both at the immediate vicinity of the larger veins and in clasts of wall–rock within brecciated veins (Malvicini, 1978; Silver Standard Resources Inc., 2011). Coira et al. (2000) and Paar et al. (2001) report silicification and phyllic to advanced argillic alterations.

3. Methods

This work is based on detailed geological mapping with structural cross–sections on the Acoite Formation to pursue the relation between the development of folds, faults and fractures and the formation of the ore–bearing veins. Systematic structural data was collected in 402 outcrops, and the statistical treatment was performed using the Openstereo software (Grohmann and Campanha, 2010).

Macroscopic description of host rocks and veins was performed at outcrops and along selected zones of drill cores containing structures and/or mineralization. Petrographic observations of selected samples used optical (transmitted and reflected) and Scanning Electron (SEM) microscopy at Universidade Federal do Rio de Janeiro (UFRJ) and at the Center for Mineral Technology (CETEM/RJ), respectively. Mineral relationships and compositions were elucidated using an FEI Quanta 400 SEM coupled to a Bruker Nano Quantax 800 EDS and an SDD XFlash 4030 detector, after spectral calibration using a copper standard. The equipment was operated at 20 kV, spot size 5, counting time of 60 s, and standardless deconvolution with Φ(ρz) ZAF correction. The instrumental analytical error (2σ) for each analysis is below 1.5%. Few X-

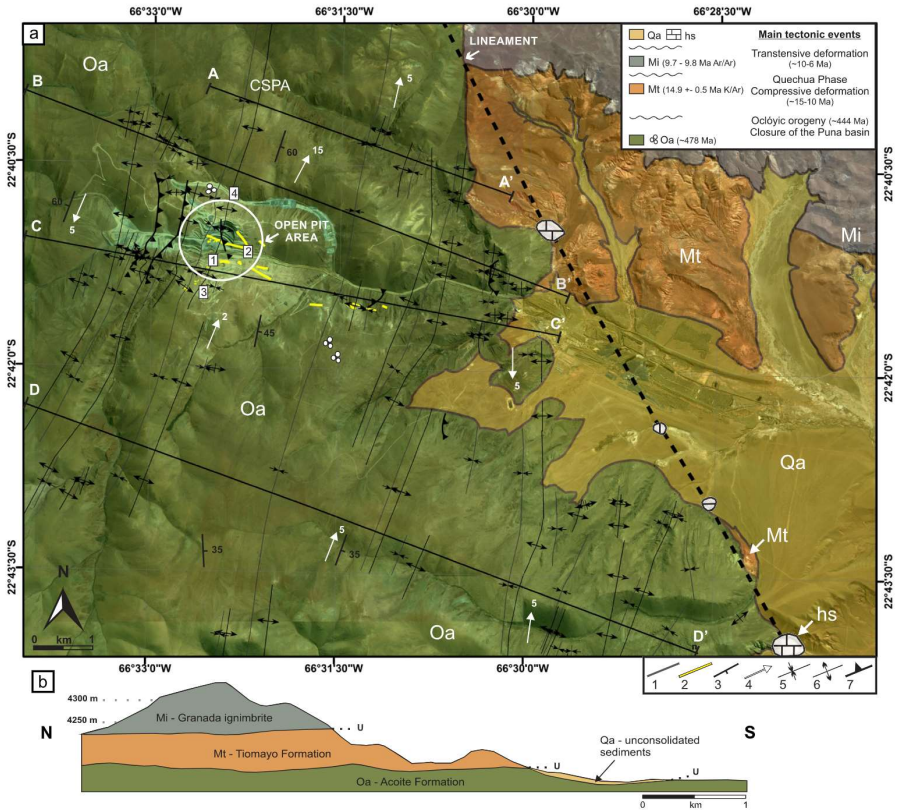

Fig. 4. Geology of the Pirquitas deposit. (A) Geological map and structural data obtained during fieldwork. Lithological units: hs– hydrothermal springs; Qa–unconsolidated sediments; Mi– Upper Miocene Granada ignimbrite (9.7–9.8 Ma Ar/Ar; Caffe et al., 2008); Mt– Middle Miocene Tiomayo Formation (14.9 ± 0.5 Ma K/Ar; Coira et al., 2004); Oa– Ordovician Acoite Formation, metasandstones and metapelites/metaconglomerates (478 Ma biostratigraphic age; Voldman et al., 2012); U – angular unconformity; CSPA – Cerro San Pedro Anticline. The numbers near the open pit area represent the main mineralized sectors, such as San Miguel (1), Potosí and Veta Blanca (2), Oploca (3) and Cortadera (4). Geological inset symbols: 1– lithological contact; 2– ore–bearing vein; 3– bedding and dip (n); 4– fold axis and plunge; 5– syncline; 6– anticline; 7– reverse fault. Cross-sections A–A′, B–B′, C–C′ and D–D′ are shown in Fig. 7 (B) Sketch of a general lithostratigraphic section along the Pirquitas deposit area.

ray diffraction (XRD) analyses were performed at CETEM for mineral identification in ore–bearing veins. We used a Bruker–AXS D4 Endeavor diffractometer with CoKα radiation (35 kV/40 mA) in the 5–80° 2θ range with a step size of 0.02° 2θ and a counting time of 1s per step.

4. Results

4.1. Stratigraphy

The oldest and most common rocks that crop out near the Pirquitas deposit are the Ordovician meta–sedimentary successions of the Acoite Formation (Figs. 4 and 5). The clastic and volcanoclastic successions of the Tiomayo Formation, the Granada ignimbrite and Quaternary unconsolidated sediments lie unconformably over the Ordovician basement. Ferruginous breccia and hydrothermal carbonate deposits are scarce in the study area.

The Acoite Formation is mostly composed of metasandstone interbedded with metapelite (Fig. 5a and b) and with scarce metaconglomerate. Metasandstone forms medium to very thick beds (10 cm to > 2 m; cf. Boggs, 2001) massive or laminated tabular strata, mostly composed of metapelite fragments, mono to polycrystalline quartz, and minor plagioclase. Sedimentary structures in metasandstone consist of ripple marks, metapelitic intraclasts (Fig. 5c), and wavy and flaser bedding (Fig. 5d). Metapelite forms very thin siltstone–claystone laminae, and locally small lenses of sulfide–rich shale, including previously recognized graptolite (e.g., Moya et al., 1994) replaced by

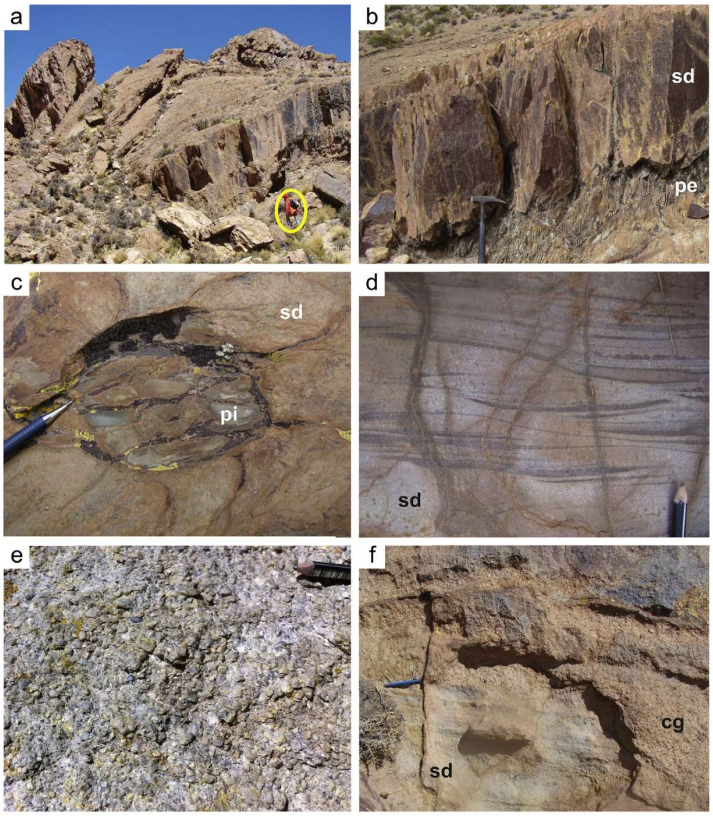

Fig. 5. Field aspects of the Acoite Formation. (A) Intercalation of metasandstone (medium to very thick beds) and metapelite tabular strata (person as scale, circle, bottom right). (B) Intercalation between metasandstone (sd) and metapelite (pe) layers (hammer as scale). Cleavage refraction between layers is observed. (C) Pelite intraclasts (pi) in metasandstone. (D) Metasandstone (sd) with flaser bedding. (E) Fine–grained metaconglomerate showing planar stratification. (F) Metaconglomerate (cg) eroding metasandstone layers (sd).

pyrite. Fine–grained (0.2–1 cm) metaconglomerate is found in medium to very thick lenses (< 2 m) with planar stratification, locally filling erosive channels on the underlying sandstones (Fig. 5e and f).

The mid-Miocene Tiomayo Formation covers the Acoite Formation in angular unconformity. At the Pirquitas area, the lower portion of the Tiomayo Formation crops out, and comprises thick reddish massive tabular strata (Fig. 6a) of sandstone and polymictic conglomerate, including metasandstone and metapelite intraclasts of the Acoite Formation. In the northern portion of the study area, an ignimbrite plateau of upper Miocene age – related to the Granada Volcano (Fig. 6a and b) – lies at angular unconformity over the Tiomayo and Acoite formations.

Massive layers of iron–rich polymictic breccia, probably of Quaternary age, vary from 4 to 10 m thick and cover the Acoite Formation at angular unconformity. The breccias are composed of angular and rounded pebble to boulder–sized fragments of metasandstones and metapelites derived from the Acoite Formation and iron–rich cement found mostly in low topographic areas, near current drainages.

Active hydrothermal springs form oval–shaped deposits of up to 7 m diameter that discharge hot water and gases (Fig. 6c and d) accompanied by white–colored carbonate deposition. These deposits occur lie the NW–SE lineament to the east of the open pit (Fig. 4).

4.2. Structural geology

Stereograms and rose diagrams for the collected structural data are shown in Fig. 7a. The Acoite Formation succession shows km-scale, NNE–SSW–trending folds with sub–horizontal fold–hinge lines plunging to NNE or SSW, which indicate WNW–ESE sub–horizontal shortening. These are usually asymmetrical folds with steeply dipping axial surfaces, as it can be observed in the NW-SE structural sections (Fig. 7b). East–vergent folds include the Cerro San Pedro anticline (CSPA, Figs. 7b and 8a), near the open pit area, whereas west–vergent folds are mostly

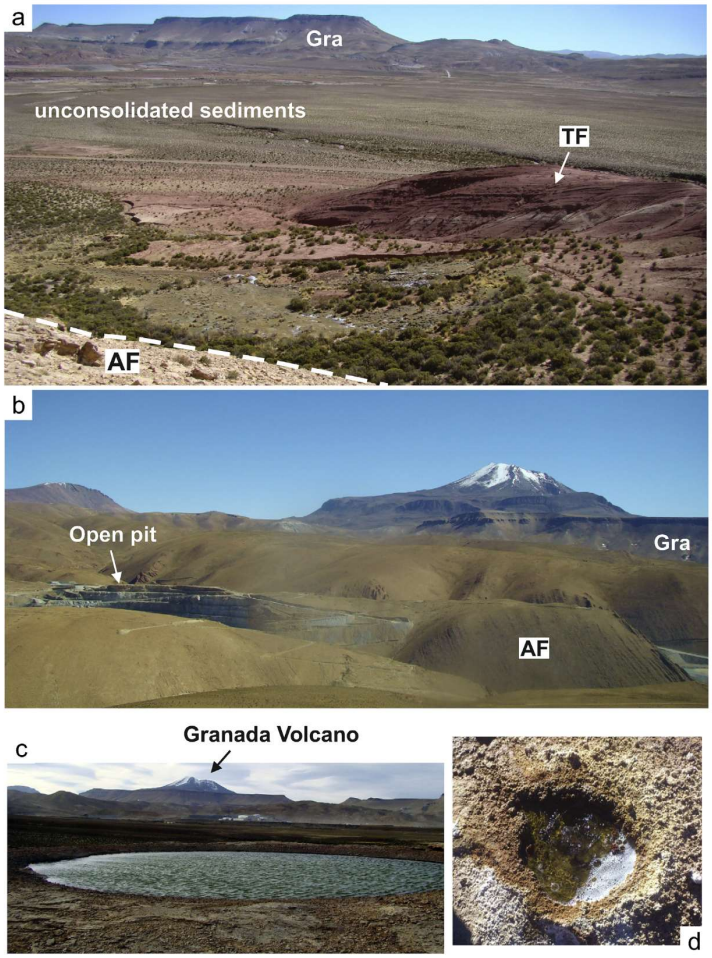

Fig. 6. Field aspects of the Tiomayo Formation, the Granada Ignimbrite and the hydrothermal springs. (A) View of stratigraphic relations between the Acoite (AF) and Tiomayo (TF) Formations, the Granada ignimbrite (Gra) plateau and unconsolidated sediments. (B) Angular unconformity between the flat Granada ignimbrite (Gra) plateau and the folded rocks of the Acoite Formation (AF). Picture was taken near the open pit area, with the Granada volcano in the background. (C, D) Active hydrothermal springs discharging hot water and gases associated to carbonate deposition within the Pirquitas deposit area. Note the Granada volcano and its associated ignimbrite plateau in the background of (C).

located to the west of the open pit. Folds are mostly open and concentric (Fig. 8b), but tight kink bands, chevron and box–folds (Fig. 8c) are also observed.

The folding of the Acoite Formation resulted in the local redistribution of minerals by pressure solution processes. The slaty cleavage planes in metapelites (< 1 mm) are marked by the crystallization of fine–grained micaceous material, as well as quartz and pyrite. Their steeply-dipping planes in metapelites are subparallel to the axial surfaces of the first–order folds, while S_1 foliation in metasandstones displays a spaced convergent fan.

Striae (L_{1f}) observed on sedimentary bedding planes (S_0) dips to NW and SE at a high angle with the fold–hinge lines and the bedding–cleavage intersection lineation (L_1). These structures, associated with preserved bed thickness of a layered succession with strong mechanical anisotropy (i.e., intercalation of metapelites and quartzites), the parallel style (class 1 B) of the folds, and the presence of different fold

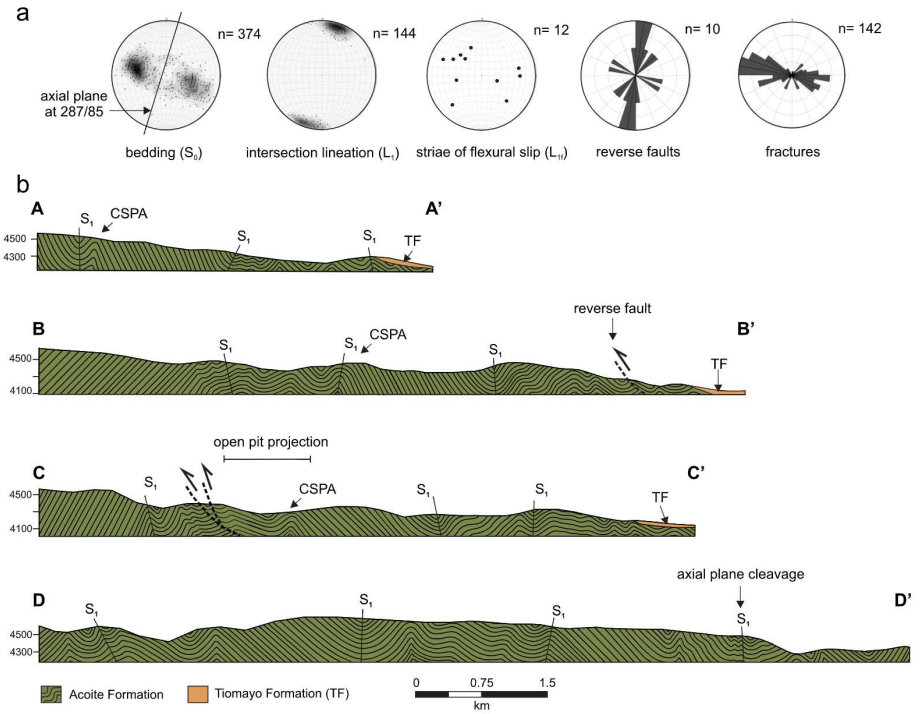

Fig. 7. Structural aspects of the Pirquitas deposit area. (A) Stereograms and rose diagrams. Lower hemisphere equal–area stereograms shows poles of sedimentary bedding (S0) planes, intersection lineation (L1) and flexural-slip-related striae (L1f). Density curves are applied with the Fisher distribution when n > 30. The rose diagram shows the orientation of reverse fault planes and fractures. (B) NW–SE structural sections (A–A′, B–B′, C–C′ and D–D′, see location in Fig. 4) along the Acoite and Tiomayo formations. Folds, axial plane slaty cleavage (S1) and reverse fault planes are represented, as well as the open pit projection.

shapes, as chevron and box–folds, may indicate flexural slip folding mechanism (e.g., Tanner, 1989; Fossen, 2016).

Although it is challenging to identify fault planes in the homogeneous meta–sedimentary succession, reverse and normal faults were locally observed or inferred by sedimentary bed truncations. Reverse faults are mostly west– and minor east–vergent, with few to dozens of meters of offset, and crosscut the bedding planes (Fig. 8, d1-d2 and e1-e2). Reverse faults within or sub–parallel to the bedding planes are also recognized. Ramp–flat geometry and characteristic anticlines on the hanging wall were recognized at several outcrops. Normal faults are scarce, show few meters of offset, and usually develop tectonic breccia.

Subvertical fracture planes are widely distributed in the Acoite Formation. They are represented by 1–10 mm-wide open fractures or up to 10 cm-wide veins. The latter is usually associated with iron–rich material, microbreccias and clay minerals, and locally with ore minerals. Two main sets of joints were individualized. They compose a conjugate fracture system at the Pirquitas deposit, dipping to NNE and SSW, and the main strike of 264° is shown in rose diagram (Fig. 7a).

4.3. Host rocks, veins, stockworks, and breccia

Fieldwork, drillcore descriptions, and petrographic analyses of selected samples allowed the individualization of the mineralogical and textural assemblages related to different depositional stages at the Pirquitas deposit. A population of euhedral and compositionally homogeneous pyrite crystals (~1 μm) was observed via SEM-EDS. It forms aggregates (< 2 mm) that are observed conformably with the bedding of the meta–sedimentary host rocks. Pyrite crystals are found regionally in the Acoite Formation and may represent diagenetic sulfide crystallized from sulfate reduction processes. These pyrite aggregates, as well as quartz, are locally recrystallized along the S_1 slaty cleavage planes, and are not associated with the ore–bearing assemblages.

4.3.1. Barren veins and stockworks (type–I)

Tabular, massive and low–sulfide content (ca. 1%) quartz veins are nearly continuous, vary in width from 0.5 to 3 m, and extend up to dozens of meters. They are mostly parallel (locally discordant) to the sedimentary bedding of the Acoite Formation and frequently occur in the hinge zone of anticlines (Fig. 9a and b). N–S quartz–pyrite vein zone with jigsaw puzzle breccia (Fig. 9c and d), displaying an E–W trending orientation crops out only locally to the west of the Pirquitas deposit. Both veins and jigsaw puzzle breccia of type–I are composed of milky quartz, with high amounts of intracrystalline defects. They are barren, whereas non–economic, very low gold contents have been locally

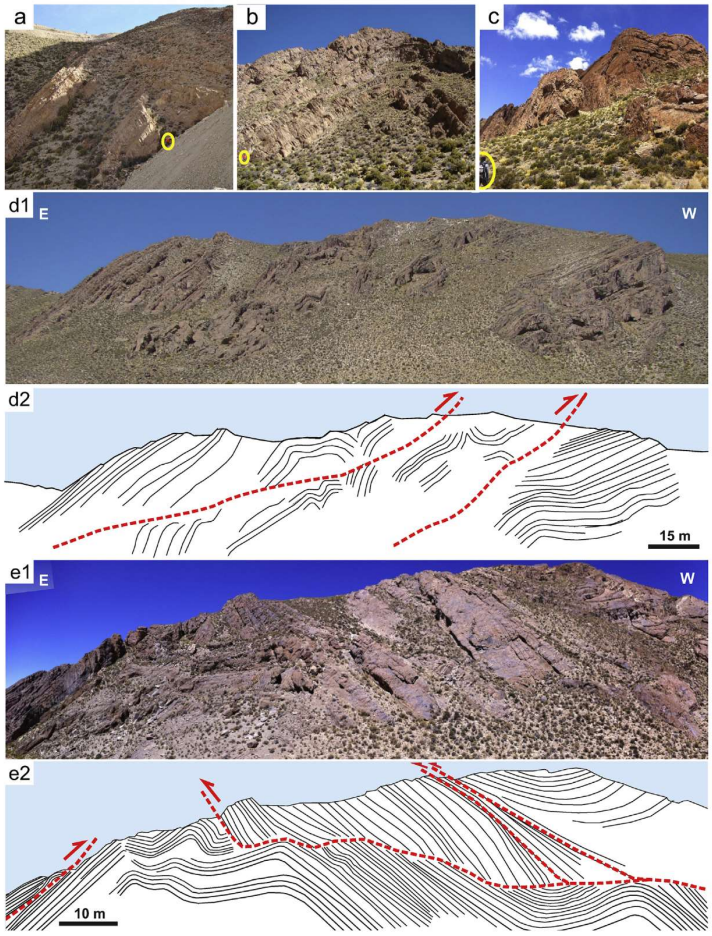

Fig. 8. Field aspects of folding and faulting in the Acoite Formation. (A) Assymetrical east–vergent Cerro San Pedro anticline – CSPA (person as scale, circle, bottom right). (B) Symmetrical open fold with subvertical axial plane (person as scale, circle, bottom left). (C) Box-fold (person as scale, circle, bottom left). (D1–D2) West–vergent faults inferred from sedimentary bed truncations; (E1–E2) East–vergent reverse faults with flat ramp geometry and ramifications and west–vergent fault with anticline developed at the hanging wall.

observed.

4.3.2. Ore–bearing veins and stockworks (type–II)

Ore–bearing silver, tin, and zinc veins cross–cut barren type–I veins and are distributed in different sectors near the open pit area (Figs. 4 and 10).

Type–II veins have mostly WNW–ESE strike, are vertical to sub–vertical, continuous (Fig. 9e), with tabular or lenticular geometry. Exploitation was focused on the San Miguel and Potosí sectors. At the San Miguel sector, tabular to lenticular, massive quartz–pyrite veins predominate, mostly thinner than 15 cm, which constitutes a sheeted vein system (Fig. 9f) of approximately 120 m width. The predominant vein textures at Potosí and Veta Blanca sectors are colloform to crustiform (Fig. 11a), with compositional banding composed of intercalation of quartz, botryoidal pyrite, sphalerite, galena, and Ag–Sn sulfides (see below). The Cortadera sector shows the predominance of both breccia and colloform veins composed of pyrite (including botryoidal type), sphalerite, galena, and quartz (Fig. 11b–d). Quartz breccia (Fig. 11e) and stockworks usually contain medium to high sulfide content, mostly pyrite. The host rocks and quartz–pyrite veins are

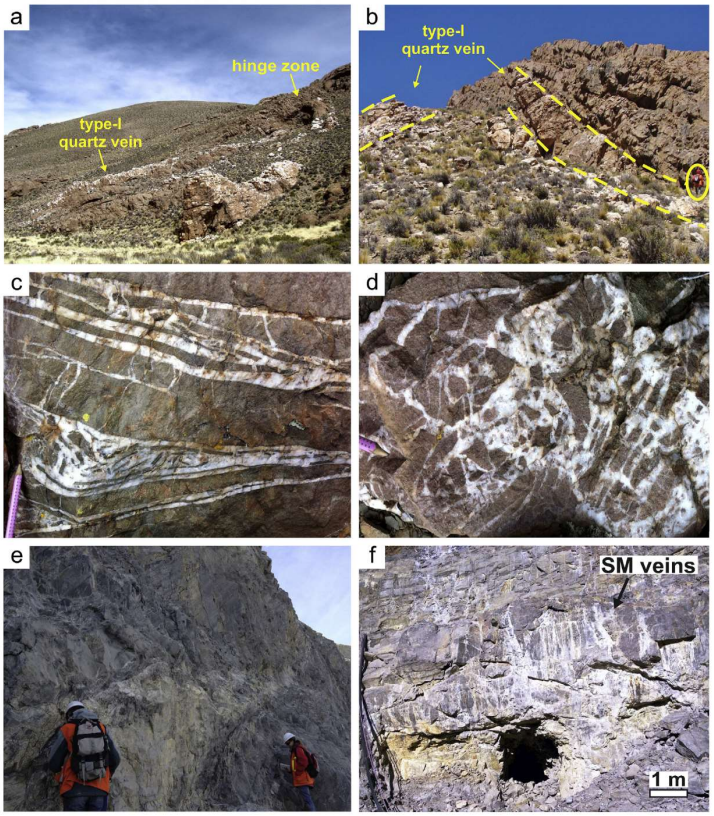

Fig. 9. Vein types at Mina Pirquitas. (A and B) Tabular, massive, barren type–I quartz veins parallel to the sedimentary bedding of the folded Acoite Formation (person as scale at B, circle, bottom right). (C) Barren type–I quartz veins. (D) Jigsaw puzzle breccia. (E) Subvertical, tabular, continuous type-II vein at Potosí sector, nearby the open pit. (F) San Miguel sheeted vein system in the open pit. Note an old artisanal mining adit.

cross–cut by massive veins and veinlets (Fig. 11f). These are mostly composed of pyrite, arsenopyrite, sphalerite, and quartz, locally associated with centimetric normal and reverse faults (Fig. 11g).

Argentite occurs as inclusions in arsenian pyrite/arsenopyrite (with 7.72 wt% Ag) and as individual crystals (with 7.42 wt% Ag) bordering stannite and pyrite (Fig. 11h and i). Stannite occurs as inclusions or bordering pyrite/arsenopyrite crystals. It contains freibergite inclusions (with 5.76 wt% Ag) and locally native silver (Fig. 11j and k). These veinlets also contain inclusions of cassiterite. The veins above described and veinlets are cross–cut by several stages of colloform quartz–pyrite–sphalerite–galena (and associated anglesite) veins, locally with variable amounts of dickite and ordinary kaolinite. Sulfide–arsenide immiscible inclusions in galena crystals show Ag, Sb, and As contents. The colloform textures represent open–space fillings during multiple stages of fracturing, as evidenced by cross–cutting relations. Other minerals identified by SEM and XRD comprise F–Ba–rich goyazite, tosudite, xenotime, and Pb–Ba–Ca–sulfates of the alunite group.

4.3.3. Ore–bearing hydrothermal breccia

Hydrothermal matrix–supported polymictic breccia were observed near the open pit area in the Potosí and Oploca sectors, and individualized based on their framework and matrix composition. The first type has angular fragments of metapelite and metasandstone from the Acoite Formation immersed in a matrix composed of massive pyrite, minor sphalerite, and quartz as gangue. The second stage of sphalerite crystallization, as well as galena, represents the last ore–infilling stage within the pyrite–dominant matrix (Fig. 12a).

The framework of the second breccia type includes fragments of meta–sedimentary host rocks, very fine grained volcanic rocks, porphyritic dacite, and monocrystalline and polycrystalline quartz. Metapelite and metasandstone clasts are sub–angular, vary in size from sand to cobble, and show incipient inherited foliation. Dacite fragments (Fig. 12b) show abundant quartz and plagioclase phenocrysts, the latter usually altered to sericite. Monocrystalline quartz is found as fragments or euhedral to anhedral crystals. They locally show irregular, embayed

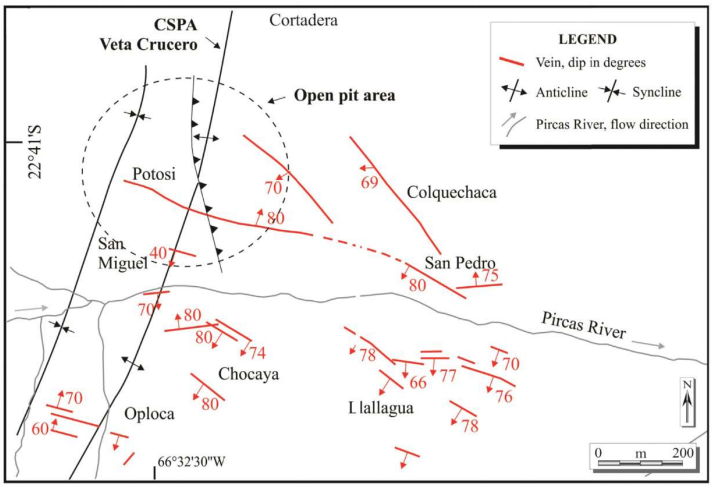

Fig. 10. Detailed map of the open pit area, showing the distribution of the mineralized sectors, see location in Fig. 4 (Based on Malvicini, 1978; Silver Standard Resources Inc., 2001, and collected field data).

or corroded borders (Fig. 12c). Pebble-sized polycrystalline quartz fragments are sub–angular, and individual crystals show undulose extinction and comb texture, typical of quartz veins (Fig. 12d). Most lithoclasts contain euhedral pyrite crystals and very fine–grained kaolinite patches (K–feldspar alteration?) that are crosscut by fractures filled with galena. The matrix shows pyrite, sphalerite, and galena in aggregates or as individual crystals. Pyrite aggregates locally show fractures filled with sphalerite and galena (Fig. 12e). The latter infill the inner fracture zones, or border pyrite and sphalerite crystals. Pyrite crystals with arsenopyrite inclusions (Fig. 12f) predominate volumetrically over the other individual crystals of opaque minerals in the matrix. Low–Fe sphalerite and galena frequently show corroded crystals, and arsenopyrite with low–Sb contents (sulfosalt?) shows exsolution textures within its host galena crystals (Fig. 12g).

5. Discussion

5.1. Ordovician deformation

The Early Ordovician Acoite Formation hosts the Pirquitas deposit and comprises successions of metasandstone and metapelite with ripple marks, wavy and flaser bedding, and fine–grained conglomerate lenses filling erosive channels. The sedimentary structures are interpreted here as registers of a lower flow regime and re-suspension of sediments as a product of turbulent flow reworking (cf. Mutti et al., 2003), which is consistent with the deposition in a turbidite system, as interpreted by Bahlburg (1990, 1998). The structural data on the Acoite Formation suggest the contemporaneous formation of folds, west–vergent and minor east–vergent reverse faults, WNW–ESE fracture planes and barren type–I quartz veins during Late Ordovician–Early Silurian times. Plots of the structural data obtained on axial surfaces, faults, and sets of fractures indicate coincident WNW–ESE orientation of the sub–horizontal σ1 (Fig. 13a and b). Flexural slip folding and barren saddle–type (type–I) vein formation is associated with folding amplification during the compressional stage. The intensity and style of the deformation described in the Acoite Formation, such as regional–scale open to tight folds, chevron folds, ramp–flat geometry with anticlines associated, and the scarce occurrence of normal faults, are consistent with those previously described as a result of the Oclóyic orogeny in the Central Andes (e.g., Thomas and Astini, 2007). According to Mon and Salfity (1995), the intense folding generated during this orogenic event also developed faults and shear zones that began along a basal décollement. Basal décollements, fault-bend-fold, and fold-bend-fold deformation styles have been recently identified at the Pirquitas mine region by Rojas Vera et al. (2019), based on surface geology, seismics (well data) and software-based structural modeling. The lack of major thrusts and reverse faults in the study area could indicate the existence of detachment folds or fault–propagation folds related to blind faults connected to a basal décollement.

5.2. Middle to upper Miocene: the Quechua phase of the Andean Orogeny and contemporaneous volcanism

The mid Miocene is considered the metallogenetic epoch in the northern Puna, due to spatial and temporal links between ore deposits and 16 to 12 Ma volcanic domes and dacitic stocks (Caffe and Coira, 1999; Caffe et al., 2002). During this time interval, the northern Puna was assumed to be under a compressional regime related to the Quechua phase of the Andean Orogeny (ca. 15 to 10 Ma; Cladouhos et al., 1994). According to Cladouhos et al. (1994), reverse faulting and minor folding were generated by the Quechua phase, and that deformation younger than 9 Ma is on normal and strike-slip faults that indicate diverse Plio-Quaternary strain orientations.

According to Cladouhos et al. (1994), fault kinematics from the northern Puna region before ca. 9 Ma involved thrusting on NNE-SSW striking faults, which produced an average shortening direction of 120° ± 20°.

Available geochronological data indicate that the deposition of the Tiomayo Formation (14.9 ± 0.5 to 12.1 ± 0.7 Ma; Coira et al., 2004) was partly contemporaneous with the Andean Orogeny. This succession lies in unconformity on the Acoite Formation and shows evidence of low deformation intensity such as ample homoclines, open folds (axis

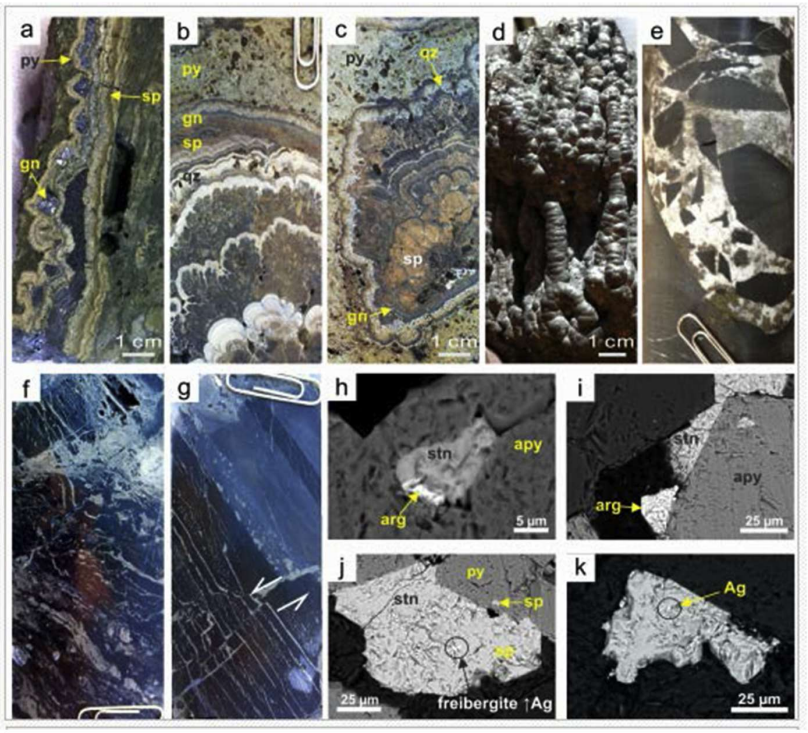

Fig. 11. Macroscopic and microscopic aspects of ore–bearing veins (type–II). (A) Colloform texture of the Potosí vein. (B–C) Cortadera colloform vein composed of pyrite–sphalerite–galena and quartz bands. (D) Botryoidal pyrite. (E) Quartz–pyrite breccias. (F) Massive pyrite veins and veinlets cross–cutting the metasedimentary host rock. (G) Normal fault plane filled with pyrite. (H) Argentite inclusion in stannite. (I) Argentite crystals bordering stannite and pyrite. (J) Stannite bordering pyrite/arsenopyrite crystals with freibergite inclusion. (K) Inclusion of native silver in stannite crystal. Py = pyrite, sp = sphalerite, gn = galena, qz = quartz, stn = stannite, apy = arsenopyrite, arg = argentite, Ag = silver. A to H are drill cores, H to K are backscattered SEM images.

plunging towards North or South at a low angle) and normal faults, both at the Pirquitas deposit and elsewhere in the Puna region (Coira et al., 2004). The structures described in the field are taken as evidence that the Tiomayo Formation was affected by a deformational event, probably associated with the Quechua Phase, which is not compatible with structures developed during the Ordovician Oclóyic Orogeny, both in terms of timing and deformational pattern.

Similarly, the upper Miocene volcanic activity at the Puna region (ca. 10 to 6 Ma; De Silva, 1989; Coira and Kay, 2004) overlaps the time interval attributed to the Quechua Phase. As pointed by Riller et al. (2001) and Holdsworth et al. (1997), a series of regional–scale, NW–SE fault zones (Fig. 2) represents Paleozoic structures that were reactivated as left–lateral transtensional faults during the Cenozoic. Those authors consider that regional, upper–crust dilation favored the volcanic activity after ca. 10 million years ago (i.e., registered as collapse calderas, domes, dykes, vents, and hydrothermal alteration) along with regional–scale structures, via channeling and accumulation of large amounts of magma and interaction between magmatic and meteoric fluids. Thus, we interpret that NW–SE and WNW–ESE ore–bearing veins of the Pirquitas deposit represent, respectively, second–order R– and T–fractures associated with major regional–scale, sinistral, brittle shear zones such as the Lípez and the Olacapato–El Toro faults. In this sense, the Granada volcano is linearly linked to the Coranzuli caldera (ca. 6.6 Ma; Caffe et al., 2002) and active hydrothermal carbonate springs along a 40 km long NW–SE lineament (Fig. 13c), which are interpreted here as an extension of the NW–SE Lípez fault (Fig. 1).

Indeed, the Granada volcano (i.e., the 9.8 to 9.7 Ma Granada ignimbrite; Caffe et al., 2008), breccia pipes at the deposit area, and possibly subordinate intrusions nearby may be the best candidates for metal and magmatic fluid component suppliers to the Pirquitas deposit. As reported elsewhere (e.g., Corbett, 2005), hydrothermal fluids can travel long distances, mostly if fault–valve behavior is active along brittle faults (e.g., Sibson et al., 1975; Sibson, 1994) in association with assumed magmatic activity in depth (e.g., Sillitoe and Hedenquist, 2003). Magmatic and meteoric fluids would then mix with meteoric fluids along those faults promoting channelized diffusion of hydrothermal cells.

The coinciding strike between Ordovician subvertical fractures and WNW–ESE ore–bearing veins (type–II) suggests the reactivation of Paleozoic structures. Field and petrographic observations, and the

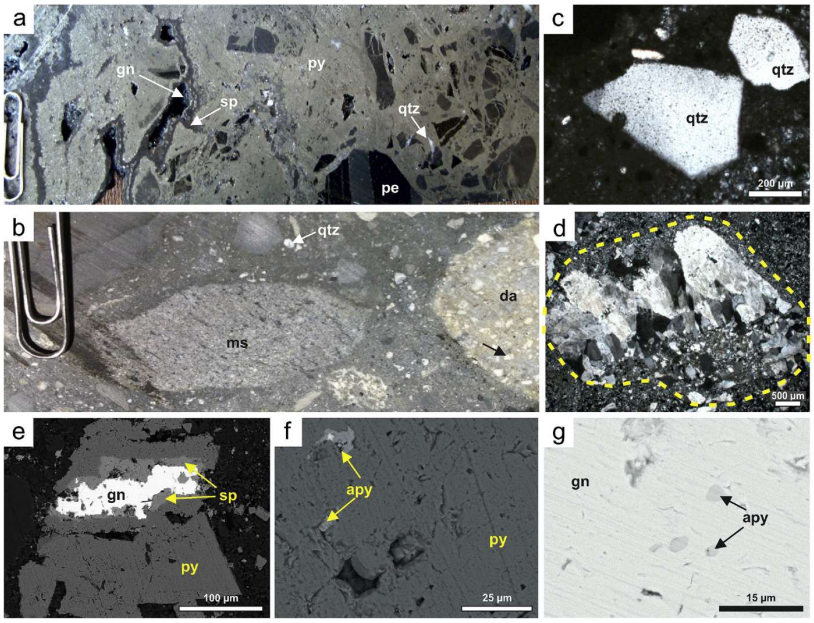

Fig. 12. Macroscopic and microscopic aspects of hydrothermal breccia. (A) Drill core image of matrix–supported polymictic breccia with angular fragments of metapelites (pe) and metasandstones from the Acoite Formation immersed in a matrix composed by massive pyrite (py), minor sphalerite (sp), galena (gn) and quartz (qtz). (B) Drill core image of matrix–supported polymictic breccia with metassedimentary rocks (ms), dacite (da) and quartz fragments (qtz). Note altered feldspar crystals in the dacite fragment (arrow). (C) Photomicrography (PL) of embayed border of monocrystalline quartz fragments. (D) Photomicrography (PL) of fragments of quartz vein with comb texture. Borders of the fragment is indicated by the dashed line. (E–G) are backscattered SEM images. (E) Pyrite (py) aggregate with fracture filled with sphalerite (sp) and galena (gn). (F) Arsenopyrite (apy) inclusions in pyrite crystal (py). (G) Immiscible inclusions of arsenopyrite (apy) in galena (gn) crystal.

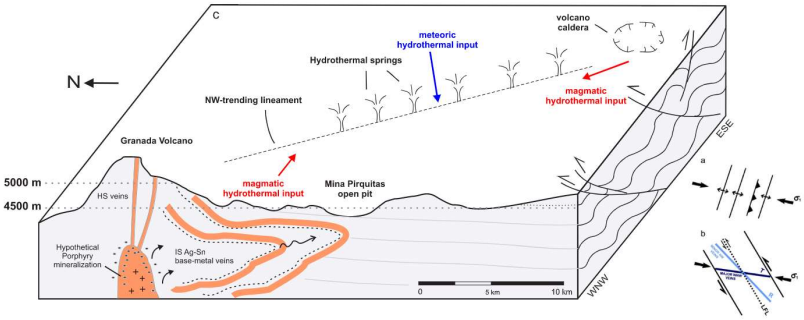

Fig. 13. Schematic diagram showing the structural evolution of the Pirquitas region and the proposed link between regional structures, the Granada volcano and the Corazuli caldera and hydrothermal fluids. (A) Folding during the Oclóyic Orogeny. (B) NW–SE and WNW–ESE ore–bearing veins of the Pirquitas deposit interpreted as R and T shears fractures developed during the Quechua deformation phase, which is paralell with the López Fault, a major regional–scale sinistral brittle shear zone. LFL: López Fault Lineament. (C) Schematic diagram showing the hydrothermal springs related to the NW-SE lineament between the Granada volcano and the Coranzuli caldera. It is proposed a hydrothermal fluid migration, represented in part by an epithermal system of intermediate sulfidation (IS) type, with fluid–source probably related to the activity of the Granada volcano or other hidden subvolcanic intrusions, that would interact with hydrothermal fluids of shallow meteoric origin along regional structures. Schematic possibility for the occurrence of high sulfidation epithermal and porphyry mineralization is also represented.

crosscutting relation between the Potosí vein system and older thrust zones at the open pit area also support this assumption (Fig. 4). Exploration data shows high–grade Ag–Zn mineralization in quartz veins at the hinge zone of the Cerro San Pedro anticline (CSPA; Figs. 4 and 10) in comparison with the surrounding areas (Mina Pirquitas staff, pers. comm.). This structure was identified during underground exploration and named as Veta Crucero ('Crossed Vein'). Considering the Oclóyic deformation and related veins, the Veta Crucero probably developed at the intersection of an NNE–striking quartz vein (type–I) and the WNW–ESE ore–bearing veins.

Moreover, most of the ore–bearing veins show undeformed colloform and comb textures of open–space infillings, typically formed in near–surface, low–pressure environments (cf. Taylor, 2009). Jigsaw puzzle breccia (cf. Sibson, 1986) are interpreted as a result of distention induced by discrete, local slip planes along shear zones. Brecciated veins with similar textures can also develop as a result of intense fluid discharge. Sphalerite and galena show irregular/corroded textures probably related to repeated hydraulic fracturing under the same stress field, followed by a corrosive chemical process.

As summarized by Arce–Burgoa (2009), most of the Bolivian Belt deposits are epithermal of the intermediate–sulfidation subtype, and structurally–controlled along regional lineaments, transcurrent faults, and local–scale tension fractures. Indeed, Simmons et al. (2005) showed that there are exceptions to the general environments of formation for ore deposits considered as epithermal, including association with magmas from outside conventional volcanic arcs, location in areas under transpressive tectonic regimes or in crustal zones where deep tensional structures develop through rifting, among others.

Based on the above arguments, we interpret that older Oclóyic structures acted as conduits for magmatic and meteoric hydrothermal fluid flow during the upper Miocene at the Pirquitas deposit. As such, Ag–Sn–Zn ore may have concentrated in intersections between Miocene brittle structures and previous folds, faults and fractures. In a regional perspective, the melting of meta-sedimentary host rocks could be the source for peraluminous, low-oxygen fugacity magmas with potential to host Sn–Ag–bearing ore, as proposed for the BTSB deposits (e.g., Cunningham et al., 1996). Melting of deeply seated units of the metasedimentary successions that host the Pirquitas Mine might have produced magmas with similar geochemical affinity and metal contents, discharging ore-bearing magmatic fluids that would interact with near–surface meteoric fluids.

6. Conclusions

The Pirquitas mine was an important producer of Ag–Sn–Zn until 2017, but scarce works on the structural geology of the deposit were carried out. Our investigation of geologic structures, coupled with compiled regional information, permits to state the following:

- The Ag–Sn–Zn ore of the Pirquitas deposit represents a structurally–controlled epithermal mineralization;
- The main deformation of the Acoite Formation meta–sedimentary host rocks is interpreted as a product of WNW–ESE sub–horizontal shortening during the Late Ordovician–Early Silurian Oclóyic orogeny (ca. 444 Ma.);
- Reactivation of the regional–scale Oclóyic structures during the upper Miocene Quechua Phase is interpreted as simultaneous with the magmatic activity in the northern Puna region, hydrothermal fluid flow and ore deposition at the Pirquitas deposit;
- The NW–SE and WNW–ESE ore–bearing veins of the Pirquitas deposit represent, respectively, second–order R– and T–fractures associated with major regional–scale, sinistral, brittle shear zones such as the Lípez and the Olacapato–El Toro faults;
- Similarities in mineralogy, structural controls, and association with magmatic activity indicate that Pirquitas is the southernmost deposit of the Bolivian Tin–Silver Belt.
- Future exploratory work searching for porphyry to epithermal deposits at the Puna region should consider the potential of the Granada Volcano, the Coranzuli Caldera and other subvolcanic intrusions along with regional structures as sources for hydrothermal fluids (magmatic + meteoric) and associated mineralization.

Acknowledgments

The authors thank the Silver Standard Resources Inc. and Mina Pirquitas Inc. staff, in particular Carlos Perez, for providing access to previous technical reports and support during fieldwork. The authors acknowledge the Center for Mineral Technology (CETEM) staff for all the support during sample preparations and analytical procedures, in particular Antonieta Middea. F.M. Passamani thanks the Coordenação de Aperfeiçoamento de Pessoal de Nível Superior – CAPES for the MSc. Scholarship in Brazil and the Programa de Apoio à Pós-Graduação – PROAP for financing part of this study. The authors also thank the contributions of the Editor Andres Folguera, two anonymous reviewers of JSAMES, and Maria de Fátima Bitencourt for their constructive comments that have enhanced the quality of the manuscript.

References

Arce–Burgoa, O., 2009. Metalliferous Ore Deposits of Bolivia: La Paz. SPC Impresores S.A.
Allmendinger, R.W., Jordan, T.E., Kay, S.M., Isacks, B.L., 1997. Evolution of Altiplano–Puna plateau of the central Andes. Annu. Rev. Earth Planet Sci. 25, 139–174.
Allmendinger, R.W., Ramos, V.A., Jordan, T.E., Palma, M., Isacks, B.L., 1983. Paleogeography and Andean structural geometry, northwest Argentina. Tectonics 2, 1–16.
Alonso, R.N., Viramonte, J., Gutiérrz, R., 1984. Puna Austral – bases para el subprovincialismo geológico de la Puna [ext. abs. In: Congreso Geológico Argentino, 9th, San Carlos de Bariloche, Argentina, 1984, Extended Abstracts, pp. 43–63.
Bahlburg, H., 1990. The Ordovician basin in the Puna of NW Argentina and N Chile: geodynamic evolution from back–arc to foreland basin. Geotekt. Forsch. 75, 1–107.
Bahlburg, H., 1998. The Geochemistry and Provenance of Ordovician Turbidites in the Argentine Puna, vol. 142. Geological Society of London, Special Publications, pp. 127–142.
Bahlburg, H., Hervé, F., 1997. Geodynamic evolution and tectonostratigraphic terranes of northwestern Argentina and northern Chile. Geol. Soc. Am. 109, 869–884.
Bahlburg, H., Breitkreuz, C., Maletz, J., Moya, M.C., Salfity, J.A., 1990. The Ordovician sedimentary rocks in the Puna of Argentina and Chile: new stratigraphical data based on graptolites. Newsl. Stratigr. 23, 69–89.
Benavides–Cáceres, V., 1999. Orogenic evolution of the Peruvian Andes: the andean cycle in skinner. In: In: BJ (Ed.), Geology and Ore Deposits of the Central Andes, vol. 7 Society of Economic Geologists Special Publication.
Boggs Jr., S., 2001. In: Principles of Sedimentology and Stratigraphy, 3ed. Prentice–Hall, Upper Saddle River, New Jersey, pp. 726.
Caffe, P.J., Coira, B.L., 1999. Complejos de domos volcánicos del Mioceno médio de Puna Norte. Un modelo geológico y metalogenético para yacimientos epitermales de metales de base ricos en plata (estaño). In: In: Zappettini, E.O. (Ed.), Recursos Minerales de la República Argentina: Boletín del Instituto de Geología y Recursos Minerales del Servicio Geológico Minero Argentino, vol. 35. pp. 1569–1578.
Caffe, P.J., Soler, M.M., Coira, B.L., Onoe, A.T., Cordani, U.G., 2008. The Granada ignimbrite: a compound pyroclastic unit and its relationship with Upper Miocene caldera volcanism in the northern Puna. J. S. Am. Earth Sci. 25, 464–484.
Caffe, P.J., Trumbull, R.B., Coira, B.L., Romer, R.L., 2002. Petrogenesis of early Neogene magmatism in the northern Puna; implications for magma genesis and crustal processes in the central andean plateau. J. Petrol. 43, 907–942.
Chernicoff, C.J., Richards, J.P., Zappettini, E.O., 2002. Crustal lineament control on magmatism and mineralization in northwestern Argentina: geological, geophysical, and remote sensing evidence. Ore Geol. Rev. 21, 127–155.
Cladouhos, T.T., Allmendinger, R.W., Coira, B., Farrar, E., 1994. Late Cenozoic deformation in the Central Andes: fault kinematics from the northern Puna, northwestern Argentina and southwestern Bolivia. J. S. Am. Earth Sci. 7, 209–228.
Coira, B., de Brodtkorb, M.K., 1995. Paragenesis of polymetallic mineralization related with Cenozoic volcanism in northern Puna Argentina. In: In: Mank, J.L., George, J.D.S. (Eds.), Pacrin Congress, vol. 95. pp. 135–140.
Coira, B.L., Kay, S.M., 2004. Central andean plateau ignimbrites in the Puna back-arc cenozoic volcanic province (PBVC) [abs.]. Int. Assoc. Volcanol. Chem. Earth's Interior, Pucón, Chile 2004 (Abstract unpaginated).
Coira, B., Caffe, P.J., Ramírez, A., Chayle, W., Díaz, A., Rosas, S.A., Pérez, A., Pérez, E.M.B., Orosco, O., Martínez, M., 2004. Descripción geológica de la Hoja 2366–I "Mina Pirquitas" a escala 1:250.000. Boletín del Instituto de Geología y Recursos Minerales del Servicio Geológico Minero Argentino 269, 1–123.
Coira, B., Chayle, W., Díaz, A., 2000. Chimeneas de brecha del yacimiento polimetálico de Sn Ag Mina Pirquitas. Un testimonio de sus raíces subvolcánicas [ext. abs. In: Congreso Geológico Boliviano, 14th, La Paz, Bolivia, vol. 2000. Extended Abstracts, pp. 357–361.

Corbett, G., 2005. In: Epithermal Au–Ag Deposit Types – Implications for Exploration: Proexplo Conference, Peru, (published on CD).
Coutand, I., Cobbold, P.R., de Urreiztieta, M., Gautier, P., Chauvin, A., Gapais, D., Rossello, E.A., López–Gamundí, O., 2001. Style and history of Andean deformation, Puna plateau, northwestern Argentina. Tectonics 20, 210–234.
Cunningham, C.G., McNamee, J., Pinto Vasquez, J., Ericksen, G.E., 1991. A model of volcanic dome-hosted precious metal deposits. Econ. Geol. 86, 415–421.
Cunningham, C.G., Zartman, R.E., McKee, E.H., Rye, R.O., Naeser, C.W., Sanjinés, O., Ericksen, G.E., Tavera, F.V., 1996. The age and thermal history of Cerro Rico de Potosi, Bolivia. Miner. Deposita 31, 374–385.
Desanois, L., Lüdersa, V., Niedermanna, S., Trumbull, R.B., 2019. Formation of epi-thermal Sn-Ag-(Zn) vein-type mineralization at the Pirquitas deposit, NW Argentina: fluid inclusion and noble gas isotopic constraints. Chem. Geol. 508, 78–91.
De Silva, S.L., 1989. Altiplano–Puna volcanic complex of the central Andes. Geology 17, 1102–1106.
Do Campo, M., Nieto, F., Albanesi, G.L., Ortega, G., Monaldi, R., 2017. Outlining the thermal posdepositional evolution of the Ordovician successions of northwestern Argentina by clay mineral analysis. chlorite geothermometry and Kübler index: Andean Geol. 44 (2), 179–212.
Dietrich, A., Lehmann, B., Wallianos, A., 2000. Bulk rock and melt inclusion geochemistry of Bolivian tin porphyry systems. Econ. Geol. 95, 313–326.
Fossen, H., 2016. Structural Geology, second ed. Cambridge University Press, pp. 524.
Grohmann, C.H., Campanha, G.A.C., 2010. OpenStereo: Open Source, Cross–Platform Software for Structural Geology Analysis [abs. American Geophysical Union Fall Meeting, California, United States Abstract IN31C-06.
Gubbels, T.L., Isacks, B.L., Farrar, E., 1993. High level surfaces, plateau uplift, and foreland development. Central Bolivian Andes: Geology 21, 695–698.
Holdsworth, R.E., Butler, C.A., Roberts, A.M., 1997. The recognition of reactivation during continental deformation. J. Geol. Soc. 154, 73–78.
Isacks, B.L., 1988. Uplift of the central andean plateau and bending of the Bolivian orocline. J. Geophys. Res. 93, 3211–3231.
Ishihara, S., 1977. The magnetite-series and ilmenite-series granitic rocks. Min. Geol. 27, 293–305.
Jacobs Engineering Group Inc, 1999. Feasibility Study Pirquitas Silver–Tin Project (Unpublished results). California, Jacobs Engineering Group Inc, Jujuy Province, Argentina.
Jordan, T.E., Isacks, B.L., Allmendinger, R.W., Brewer, J.A., Ramos, V.A., Ando, C.J., 1983. Andean tectonics related to geometry of subducted Nazca plate. Geol. Soc. Am. Bull. 94, 341–361.
Lehmann, B., 1994. Petrochemical factors governing the metallogeny of the Bolivian tin belt. In: Reutter, K.-J., Scheuber, E., Wigger, P.J. (Eds.), Tectonics of the Southern Central Andes, Structure and Evolution of an Active Continental Margin. Springer-Verlag, Berlin Heidelberg, New York, pp. 317–326.
Malvicini, L., 1978. Las vetas de estaño y plata de Minas Pirquitas (Pircas), Provincia de Jujuy, República Argentina: Revista de la Asociación Argentina de Mineralogía. Petrología y Sedimentología 9, 1–25.
McBride, S.L., Robertson, C.R.R., Clark, A.H., Farrar, E., 1983. Magmatic and metallo-genetic episodes in the northern tin belt, Cordillera Real, Bolivia. Geol. Rundsch. 72, 685–713.
Mon, R., Hongn, F., 1987. Estructura del Ordovícico de la Puna. Rev. Asoc. Geol. Argent. 42, 31–38.
Mon, R., Salfity, J.A., 1995. Tectonic evolution of the Andes of northern Argentina. In: In: Tankard, A.J., Suarez, R., Welsink, H.J. (Eds.), Petroleum Basins of South America, vol. 62. American Association of Petroleum Geologists, pp. 269–283.
Moya, M.C., Malanca, S., Monteros, J.A., Cuerda, A., 1994. Bioestratigrafía del Ordovícico Inferior en la Cordillera Oriental Argentina basada en graptolitos. Rev. Esp. Palaontol. 9 (1), 91–104.
Mutti, E., Tinterri, R., Benevelli, G., di Biase, D., Cavanna, G., 2003. Deltaic, mixed and turbidite sedimentation of ancient foreland basins. Mar. Petrol. Geol. 20, 733–755.
Paar, W.H., de Brodtkorb, M.K., Sureda, R.J., Topa, D., 2001. Mineralogía y quimismo de sulfuros y sulfosales de estaño y plomo en las vetas de Mina Pirquitas, Jujuy, Argentina (22°41'S66°28'W). Rev. Geol. Chile 28, 259–268.
Paar, W.H., Miletich, R., Topa, D., Criddle, A.J., de Brodtkorb, M.K., Amthauer, G., Tippelt, G., 2000. Suredaite, PbSnS3, a new mineral species, from the Pirquitas Ag–Sn deposit, NW–Argentina. Mineral. Cryst. Struct.: Am. Mineral. 85, 1066–1075.
Passamani, F.M., 2014. Controle estrutural e mineralização do depósito de Ag-Sn-Zn da Mina Pirquitas, Noroeste da Argentina. M.Sc. thesis. Universidade Federal do Rio de Janeiro.
Rojas Vera, E.A., Giampaoli, P., Gobbo, E., Rocha, E., Olivieri, G., Figueroa, D., 2019. Structure and tectonic evolution of the Interandean and Subandean Zones of the central Andean fold–thrust belt of Bolivia. In: Horton, B., Folguera, A. (Eds.), Andean Tectonics. Elsevier, pp. 743.
Riller, U., Petrinovic, I., Ramelow, J., Strecker, M., Oncken, O., 2001. Late Cenozoic tectonism, collapse caldera and plateau formation in the central Andes. Earth Planet Sci. Lett. 188, 299–311.
Salfity, J.A., 1985. In: Lineamientos Transversales Al Rumbo Andino Em El Noroeste Argentino [ext. abs.]: Congreso Geológico Chileno, 4th, Antofagasta, Chile, vol. 1985. Extended Abstracts, pp. 119–137 2.
Sibson, R.H., 1986. Brecciation processes in fault zones: inferences from earthquake rupturing. Pure Appl. Geophys. 124, 159–175.
Sibson, R.H., 1994. Crustal Stress, Faulting and Fluid Flow, vol. 78. Geological Society of London Special Publications, pp. 69–84.
Sibson, R.H., Moore, J.McM., Rankis, A.H., 1975. Seismic pumping: a hydrothermal fluid transport mechanism. J. Geol. Soc. Lond. 131, 653–659.
Sillitoe, R.H., Halls, C., Grant, J.N., 1975. Porphyry tin deposits in Bolivia. Econ. Geol. 70, 913–927.
Sillitoe, R.H., Steele, G.B., Thompson, J.F.H., Lang, J.R., 1998. Advanced argillic litho-caps in the Bolivian tin-silver belt. Miner. Deposita 33, 539–546.
Sillitoe, R.H., Hedenquist, J., 2003. Linkages between volcanotectonic settings, ore-fluid compositions, and epithermal precious-metal deposits. In: In: Simmons, S.F., Graham, I.J. (Eds.), Volcanic, Geothermal and Ore-Forming Fluids: Rulers and Witnesses of Processes within the Earth, vol. 10. Society of Economic Geologists Special Publication, pp. 315–343.
Silver Standard Resources Inc., 2011. NI 43–101 technical report, on the Pirquitas mine, Jujuy province, Argentina: Vancouver, silver standard Resources Inc. https://www.ssrmining.com/_resources/Pirquitas_Technical_Report_Dec_23_FINAL_v2.pdf, Accessed date: 23 May 2019.
Simmons, S.T., White, N.C., John, D.A., 2005. Geological characteristics of epithermal precious and base metal deposits: economic Geology. 100th Anniversary 485–522.
Slater, E.T., 2016. The Cortaderas Zone, Pirquitas Mine, NW Argentina: an Example of Miocene Epithermal Ag-Zn-Pb-Sn Mineralization in the Andean Tin Belt. M.Sc. thesis. Laurentian University.
Soler, M.M., Iradi, P., Pérez, C., Hoyos, M., 2008. Principales aspectos de la geología, recursos y minado de Mina Pirquitas, Jujuy [ext. abs.]: Congreso Geológico Argentino, 17th, Jujuy. pp. 343–349 Argentina, Extended Abstracts.
Sureda, R.J., Galliski, M.A., Argañaraz, P., Daroca, J., 1986. Aspectos Metalogenéticos del Noroeste Argentino (Salta y Jujuy). Capricornio 1, 39–95.
Tanner, P.W.G., 1989. The flexural-slip mechanism. J. Struct. Geol. 11 (6), 635–655.
Taylor, R.G., 2009. Ore Textures: Recognition and Interpretation. Springer, Berlin.
Thomas, W.A., Astini, R.A., 2007. Vestiges of an Ordovician west–vergent thin–skinned Ocloyic thrust belt in the Argentine Precordillera, southern Central Andes. J. Struct. Geol. 29, 1369–1385.
Turneaure, F.S., 1971. The Bolivian tin–silver province. Econ. Geol. 66, 215–225.
Voldman, G.G., Albanesi, G.L., Ortega, G., Monaldi, C.R., Zeballo, F.J., Giuliano, M.E., 2012. Biostratigraphy of the Santa Rosita formation (Furongian–Tremadocian) in its type area, eastern Cordillera, NW Argentina. Geophys. Res. Abstr. 14, 3238.
Whitman, D., Isacks, B.L., Kay, S.M., 1996. Lithospheric structure and along-strike segmentation of the central Andean Plateau: Topography, tectonics, and timing. Tectonophysics 259, 29–40.